Fermi-level Shift, Electron Separation, and Plasmon Resonance Change of Ag Nanoparticle Decorated TiO_2 Under UV Light Illumination

Wenhao Zhao, [a] Liping Wen,[b] Ivan P. Parkin,[c] Xiujian Zhao,[a] Baoshun Liu[a]

[a] State Key laboratory of silicate Materials for Architectures, Wuhan University of Technology, Wuhan City, Hubei Province, P. R. China

[b]School of Environmental & Biological Engineering, Wuhan Technology and Business University, Wuhan city, Hubei province, 430065, P. R. China

[c]Department of Chemistry, Materials Chemistry Centre, University College London, London WC1H 0AJ, U.K.

ABSTRACT:

Noble metal nanoparticles are widely used as the co-catalysts for storing and separating electrons in semiconductor photocatalysis**.** Determining such ability to is important and meaningful to understand photocatalytic mechanism. Taken the Ag nanoparticles into consideration, the present research combines *in-situ* photoconductances and theoretical analysis to evaluate the Fermi-level (E_F) shift of the UV-illuminated Ag/TiO_2 system under gaseous conditions, based on which the role of the Ag nanoparticles in storing and separating electrons was discussed. It was found that the E_F of the Ag/TiO_2 locates deeper into the gap, and the temperature variation has less effect on the E_F of the Ag/TiO_2, as compared to the undecorated TiO_2. The analysis shows that ~ 46 electrons can be stored in 10 nm Ag nanoparticles under our experimental conditions, which does not change with temperatures. The electron traps in the TiO_2 can affect the electron distribution in the TiO_2 and Ag nanoparticles. It was seen that the localized surface plasmon resonance (LSPR) of the Ag nanoparticles exhibits a blue-shift under UV light illumination, which is generally ascribed to the electron storage in the Ag nanoparticles. However, we showed that the blue-shift should have nothing to do with the electron storage in the Ag nanoparticles, so it cannot be used as an indicator for evaluating the electron storage ability. The *in-situ* XPS analysis also does not support that the LSPR blue shift can connect with the reduction of the Ag_2O layer and TiO_2.

1. INTRODUCTION

Replacing fossil fuels is required to cut CO_2 emission and limit global temperature rise. Heterogeneous photocatalysis is a solution as it uses solar energy to drive chemical reactions, such as hydrogen generation,[1,2] CO_2 reduction, [3-5] pollutant removals,[6,7] and chemical reforming.[8,9] TiO_2 is a typical photocatalyst that has been widely studied for several decades.[10-12] However, the pristine TiO_2 suffers from fast carrier recombination and low photocatalytic activity. Decoration with co-catalysts is the general way to increase photocatalytic activity by changing the carrier kinetics.[13-16] The co-catalysts include oxides, sulfides, carbides, and metals. Metallic nanoparticles, such as Ag,[17] Au,[18] Pt,[19] Pd,[20] and Ru,[21] have been widely used in the photocatalysis of TiO_2 and other semiconductors. Transient studies had shown that the photoinduced electrons in TiO_2 can transfer to metallic nanoparticles in a very short time, and thus the charge carriers are effectively separated.[22,23]

The role of metallic nanoparticles in separating carriers can affect the thermodynamic property of the electrons in semiconductors and metallic nanoparticles. As electron transfer from TiO_2 to metallic nanoparticles is fast, the electron distribution in them and TiO_2 is at the thermodynamic equilibrium under steady state. The Fermi-level (E_F) of Au + TiO_2,[24,25] Ag + TiO_2,[26,27] and Au + ZnO[28] under UV light illumination had been determined by the Nernst equation through a titration method in solutions, and the result showed that the addition of Au and Ag nanoparticles could move the E_F closer to the conduction band (CB) edge of TiO_2. The E_F up-shift increases the electron reduction ability and the electron density in TiO_2, and more electrons can also be stored in metallic nanoparticles; this should be beneficial for photocatalytic reactions from the viewpoint of thermodynamics. For the plasmon metal

nanoparticles, such as Ag and Au, it had also been seen that UV light illumination leads to a blue-shift in the localized surface plasmon resonance (LSPR), which was ascribed to the electron storage in the metal nanoparticles.[25-28] However, it had been also revealed that the LSPR blue shift is not caused by the electron storage.[29]

The titration used to obtain the E_F in solutions cannot be used for gaseous conditions. Although the E_F can also be determined from scanning Kelvin probe that detects working function change,[30,31] it is difficult to be integrated in the *in-situ* experimental environments. The Ag nanoparticle decorated TiO_2 (Ag/TiO_2) materials had been used in photocatalysis and photochromism;[32-35] they should both rely on electron distribution between TiO_2 and Ag nanoparticles. The current research developed a method to study the effect of Ag decoration on the E_F of the TiO_2 under gaseous condition and at different temperatures. The *in-situ* photoconductance measurements and theoretical analysis were combined to calculate the difference between the conduction band edge and E_F of the TiO_2 (E_{CB}-E_F) and evaluate the electron storage in Ag nanoparticles for the Ag/TiO_2 under UV light illumination**.** We obtained the different result for the effect of Ag nanoparticles on the E_F and their role in storing electrons is discussed. Furthermore, it was also clarified that the LSPR blue-shift does not arise from the electron storage in the Ag nanoparticles, and also might not relate with the Ag and TiO_2 reduction.

The finding should be meaningful for understanding physiochemical properties of plasmon/semiconductor systems under UV light illumination. The method used to study the E_F and electron storage is not limited for the Ag nanoparticles and TiO_2, and can be used for the other metallic nanoparticle decorated semiconductors. In addition, heterojunction

photocatalysis was also studied to increase photocatalytic activities through separating charge carriers**,** for examples the recently studied lead-free bismuth halide perovskite nanocrystals encapsulated in a covalent organic framework,[36] Cs_4PbBr_6/TiO_2[37] and $BiVO_4/TiO_2$.[38] In principle, the method developed in the current research can be also used to study the electron separation and storage in these heterojunction structures.

2. EXPERIMENTAL SECTION

2.1. Sample preparation

The large Ag nanoparticle modified TiO_2 was prepared through photodeposition method.[39,40] 92.7 μL of 0.1 M $AgNO_3$ aqueous solution was added into the methanol aqueous solution (50 mL, 20%, v/v), and then 0.2 g of pre-milled P25 TiO_2 powder was added. After being continuously stirring for 40 min in the dark, the solution was irradiated with a 500 W Xe lamp for 2 h under constant flow of N_2. After irradiation, the precipitate was washed with deionized water for several times, and then was ultrasonically dispersed in a ϕ50 mm glass container with pure water, which was finally dried at 60 °C for 4 h in N_2. Undecorated TiO_2 samples for control experiments were also prepared according to the same procedure for the Ag/TiO_2, except that the $AgNO_3$ was not used.

2.2. Catalyst Characterization

X-ray diffraction (XRD) patterns was obtained on the Empyrean X-ray diffraction photometer (Cu Kα) to identify the crystal phase. The scanning rate is 0.05^o 2θ s^{-1}, and the accelerating voltage and current used are 15 kV and 20 mA, respectively. The specific surface area of the powder sample was tested by N_2 adsorption on a fully automated nitrogen adsorption

instrument model Micromeritics ASAP 2460 Version 3.01 (USA). Field-emission transmission electron microscope (TEM; type: JEM2100F, JEOL, Tokyo, Japan) was used to observe the morphology of the pure and Ag/TiO_2 samples. X-ray diffraction (XRD; Empyrean, PANalytical, Almelo, Netherland) was used to check the crystal structure, with the Cu Kα radiation being used as the X-ray source. The surface chemical composition of the Ag/TiO_2 sample was checked with an X-ray photoelectron spectrometer (XPS; type: VG Multilab 2000, Thermo Scientific, Waltham, U.S.A.), with an X-ray source working with the Al Kα radiation. In addition, the XPS spectra under in-situ UV light irradiation were also measured with a 375 nm UV laser being used to irradiate the sample surface from the XPS window for 15 min. The laser spot diameter is about 10 mm, which is larger than the area of the sample to be checked. The binding energies of the samples were calibrated with respect to the adventitious carbon (C1s) as a reference line at 284.8 eV. The percentage of Ag nanoparticles supported on TiO_2 was determined using Inductively Coupled Plasma Optical Emission Spectroscopy (ICP-OES, Prodigy7, LEEMAN LABS); the Ag/TiO2 was dissolved in the HNO3 solution containing trace of HF at 60 °C. UV-Vis-NIR diffusion reflectance spectra were measured by a UV-Vis-NIR spectrophotometer equipped with an optical integrating sphere in the wavelength range of 300 nm to 1300 nm (UV-2600, Shimadzu, Tokyo, Japan).

2.3. Photoconductance measurements

Photoconductances were measured in a self-designed device in methanol-contained N_2 flow according to our previous work.[41,42] a 0.05 mm wide FTO strip of a 20 mm × 20 mm FTO glass was firstly removed by laser etching, and the pure TiO_2 and Ag/TiO_2 samples were

coated over the FTO-removed area and then dried at 50 °C to form a sample coating for conductance measurement. Conductances were measured using Keithley-2450 SourceMeter with a 2 V bias voltage in two-probe mode at different temperatures. During the whole measurement, the methanol-contained N_2 atmosphere was continuously passed though the reaction chamber at a flow rate of 0.3 NL/min under the control of a flow meter (NL/min means the standard flow rate at 0 °C and 1 atm; this is the labelled flow rate unit in the flow meter, so we used this unit here). The conductance of the coatings was firstly measured in the dark for 5 min, and then was monitored under the 375 nm laser illumination for 10 min, and finally the measurement was continuing for 5 min after the laser illumination. A photodetector based on Si (843-R-USB, Newport, United states) was used to check the light intensity, which is 60 mW/cm_2 for all the measurements. In addition, the dependences of the dark conductances on temperatures were also obtained in air from 100°C to 250°C with the ramping rate of 5°C/min.

2.4. In-situ UV-Vis-NIR absorption

To measure the UV-Vis-NIR diffusion spectra under well-controlled conditions, we designed and made a closed sample cell for diffusion spectrum measurement (The detailed description in shown in Fig. S1). The cell was well matched to the integration sphere (Shimadzu 819M-PP-1.0) that is equipped in the UV-Vis spectrophotometer (UV-2600, Shimadzu, Japan). It was used to measure the diffusion reflectance spectra of the samples before and after 375 nm laser irradiation under well-controlled atmosphere and temperature, which were transferred to absorption spectra by the Shimadzu software (for the UV-2600 photospectrometer). The temperature was set at the ambient temperature and the methanol-contained N_2 was flowed

through the cell for the whole measurement. The dark absorption spectra were obtained before illumination. Then, the sample was firstly illuminated with the 375 nm laser for ~ 10 min, and absorption spectrum was measured immediately. Then, the absorption spectrum was monitored again in the dark 10 min later. After then, pure O_2 was flowed into the cell, and the UV-Vis-NIR spectra was checked to the effect of O_2.

In additional to the spectra, the single-wavelength diffusion reflectances were also measured under and after the light illumination with self-designed equipment according to our previous study.[43] Changes in diffusion reflectance at 532 nm and 1550 nm were monitored using a Newport Si-based photodetector (1936-R, Newport, United states). A 375 nm laser was used as the excitation light source; a 532 nm laser and a 1550 nm laser were used as the signal lights for detection. The methanol-contained N_2 was continuously flowing through the measurement cell. The temperature was kept unchanged at 40 °C during the measurement. The diffusion reflectance powers were firstly monitored in the dark for ~ 5 min, and then was continuously measured under the 375 nm laser illumination. After the switching-off of the laser, the reflectance power at 532 nm and 1550 nm were further measured for a while in the dark. Lastly, the high-purify O_2 was flowed through the measurement cell, and the reflectances were further monitored to see the effect of O_2.

For the above *in-situ* photoconductances, UV-Vis-NIR spectroscopic absorption spectra, *in-situ* single-wavelength diffusion reflectance measurement, high-purity N_2 was flowed through a glass bottle containing HPLC-grade liquid methanol at a rate of 0.2 NL/min to form the methanol-contained N_2 atmosphere. High-purity O_2 stream flowed through the sample cell at a speed of 0.4 NL/min was directly used as the methanol-contained O_2 atmosphere.

3. RESULTS AND DISCUSSION

3.1 Physical property characterization

The XRD patterns (Fig. S2) do not reveal the present the presence of the Ag materials due to the low loaded amount, and the ICP analysis showed that the Ag amount is 0.34 wt. %. The TEM image of the Ag/TiO_2 is shown in Fig. 1(A), and it can be seen that some spherical nanoparticles (red dash circles) are distributed among the TiO_2 nanoparticles. One spherical nanoparticle was observed by high-resolution TEM, as show in Fig. 1(B), and the (111) lattice fringes of a silver metallic nanoparticle can be seen (right-down corner); this shows that metallic Ag nanoparticles are loaded over the TiO_2 surfaces. Furthermore, the presence of the Ag elements was also confirmed by EDX elemental mapping (Fig. S3). It can be seen that the size of Ag nanoparticle of the Ag/TiO_2 is ~ 10 nm. The Ag nanoparticles tightly connect with the TiO_2 nanoparticles; this should favor a fast electron transfer between them. XPS analysis (Fig. S4) shows that the binding energy of Ag 3d peak (367.6 eV) corresponds to the Ag_2O;[44] this means that the Ag nanoparticle surfaces should be oxidized to some extent. Fig. 2 shows the UV-Vis-NIR absorption spectra of the undecorated TiO_2 and Ag/TiO_2, and it can be seen that the Ag/TiO_2 exhibits clear LSPR extinction

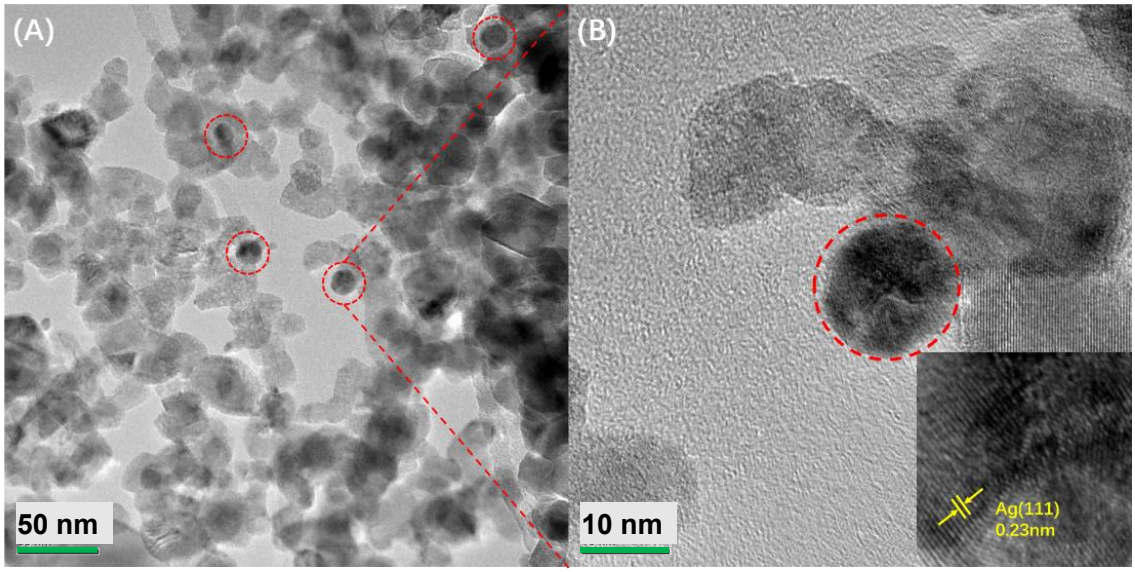

Fig. 1. TEM image (A) and high-resolution TEM image (B) of the Ag/TiO_2

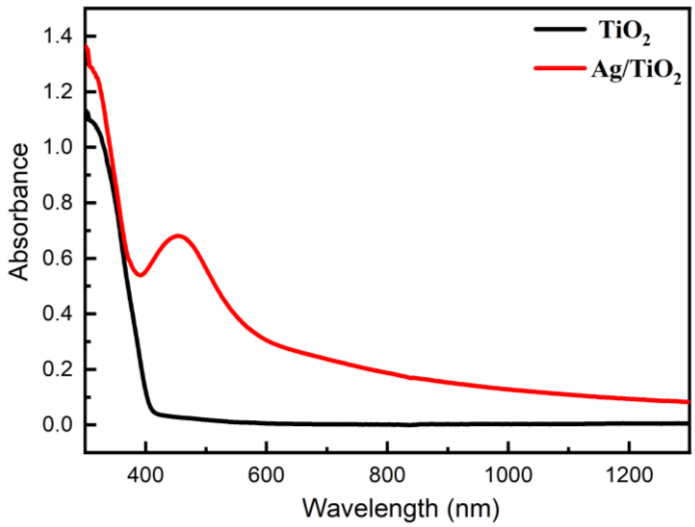

Fig. 2 UV-Vis-NIR absorption spectra of the TiO_2 and Ag/TiO_2

3.2 The effect of the Ag decoration on the Fermi energy level (E_Fs)

Fig. 3 shows the diagram of the E_F thermal equilibrium between Ag nanoparticle and TiO_2, the difference of E_F and E_{CB} can be estimated by calculating the E_F of the TiO_2, and then the electron storage in the Ag nanoparticles can be analyzed by analyzing the E_F relative change. The E_{CB} of the TiO_2 is taken as the reference level (E_{CB} = 0 eV) for simplification, and the difference between the E_{CB} and E_F (E_{CB}-E_F) is taken as the E_F here. Conductances were used

to evaluate the E_F according to the following manner. In the case of Ohmic contact (Fig. S5), the conductance is proportional to the density (n_{CB}) of the free electrons in the CB of the TiO_2 through [45]

$$\sigma = q\mu_e n_{CB} \quad (1)$$

where the μ_e is the electron mobility, q is the elementary charge. For the nano-TiO_2 used in the present research, it had been shown that the light illumination did not affect the μ_e, so the σ is considered to be proportional to n_{CB}.

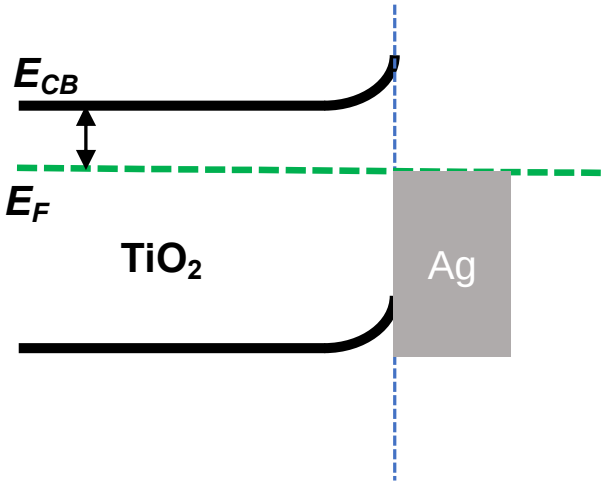

Fig. 3. Diagram of the difference between E_{CB} and E_F in the Ag/TiO_2 under the quasi equilibrium state

The conductances are used to estimates the E_{CB}-E_F for the Ag/TiO_2 and the undecorated TiO_2, which can be calculated according the following equation in the nondegenerate case.

$$E_{CB} - E_F = k_B T \ln \frac{N_{CB}}{n_{CB}} \quad (2)$$

where N_{CB} is the effective state density of the CB, k_B is the Boltzmann constant, and T is the absolute temperature. The N_{CB} is related to electron effective electron mass (m_e*) by [46]

$$N_{CB} = \frac{2(2\pi m_e^* k_B T)^{\frac{3}{2}}}{h^3} \quad (3)$$

where h is Planck constant. The m_e* of anatase TiO_2 is ~ 3 m_0 (the free electron mass).[41] The P25 also contains rutile phase that has a high m_e^*, ~ 50 m_0.[47] Thus, it is reasonable to assume that the N_{CB} is 10^{21} cm^3.

Combined with Eqns (1) and (2), the ΔE_F before and after steady light illumination is

$$E_F^p - E_F^{\mathrm{d}} = k_B T \ln \frac{\sigma_{\mathrm{p}}}{\sigma_{\mathrm{d}}} \quad (4)$$

where E_F^p (E_F^d) and σ_p (σ_d) are the E_F and conductance under steady light illumination (before light illumination), respectively. The σ is related with current through

$$I = \frac{U}{W} L d \sigma(t) \quad (5)$$

Fig. 4 shows the diagram for the current measurement. The W, L, and d in the eqn (5) correspond to the strip width, the strip length, and the thickness of the TiO_2 coating. U and I are the applied electric voltage across the TiO_2 coating and the measured current, respectively. The μ_e of the CB electrons is taken as 0.1 cm^2 V^{-1} s^{-1} .[48] The dark currents of the TiO_2 and Ag/TiO_2 at 20, 40, 60, and 80 °C were obtained from an extrapolation of Arrhenius plots (Fig. S6). The dark n_{CB} of the TiO_2 and Ag/TiO_2 were considered to be the same, which are 1.53 × 10^8 cm^{-3}, 7.8 × 10^8, 3.2 × 10^9, and 1.0 × 10^{10} cm^{-3} at 20, 40, 60, and 80 °C**,** respectively. The low n_{CB} of the undecorated TiO_2 and Ag/TiO_2 is ascribed to the electron depletion by O_2 surface chemisorption.[49,50]

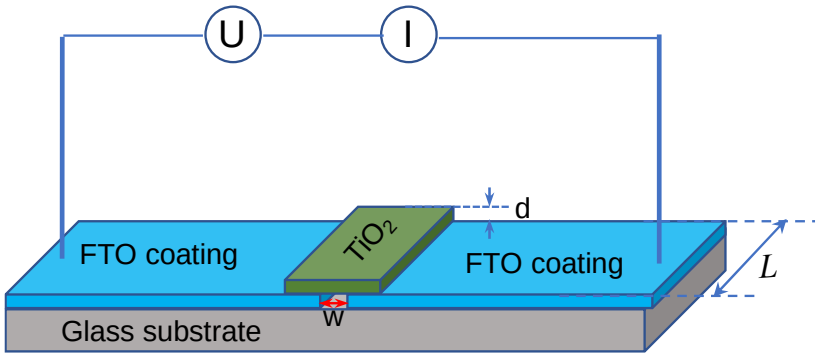

Fig. 4 Diagram of the current measurement of the TiO_2 and Ag/TiO_2

The currents of the undecorated TiO_2 and Ag/TiO_2 under and after light illumination were measured in methanol-contained N_2, as shown in Fig. 5A and B. It can be seen that the steady state photocurrents decrease and increase with the temperatures for the TiO_2 and Ag/TiO_2, respectively. Assumed that the N_{CB} of the TiO_2 is 10^{21} cm^{-3}, the steady-state E_F (relative to the E_{CB}) at different temperatures under light illumination was calculated by Eqns (2) and (4), as shown in Fig. 6. The result shows that the E_F of the undecorated TiO_2 is closer to the E_{CB} of TiO_2 as compared to the Ag/TiO_2 at all temperatures. Increasing temperature from 20 °C to 80 °C leads to a decrease of the E_F for the undecorated TiO_2 from 0.23 to 0.28 eV below the E_{CB}, but has less effect on E_F for Ag/TiO_2.

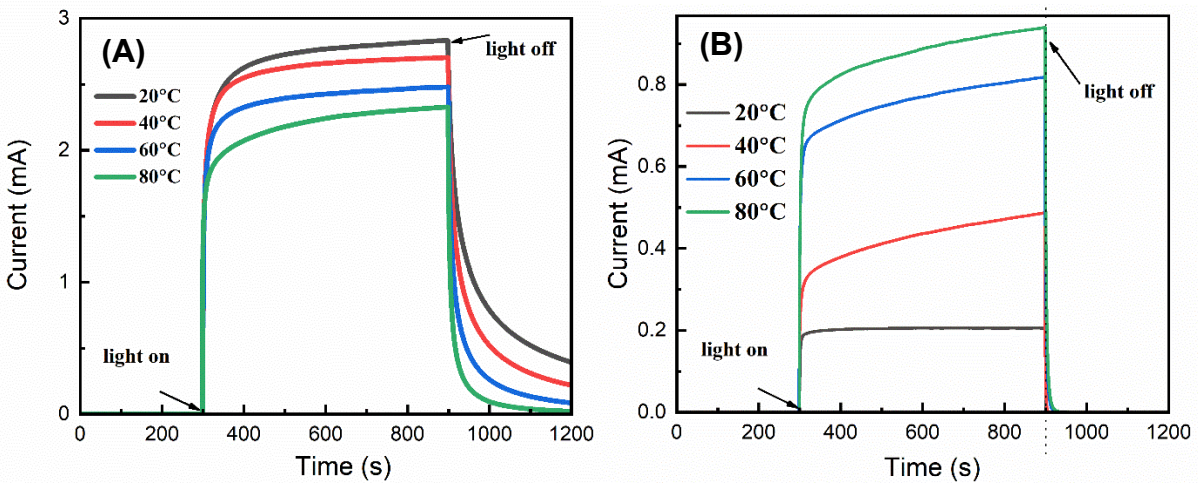

Fig. 5. Photocurrents of the TiO_2 (A) and Ag/TiO_2 (B) measured at different temperatures under 375 nm laser excitation in the presence of methanol-containing N_2.

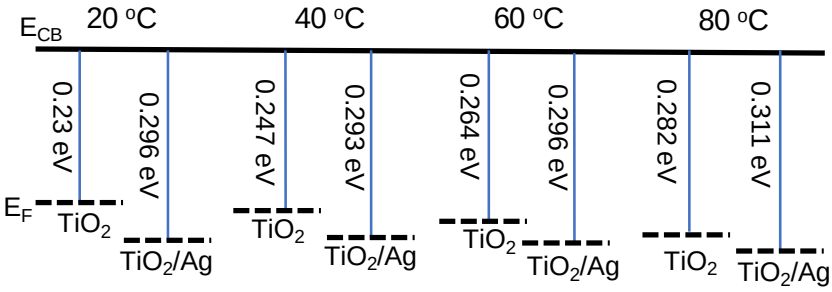

Fig. 6 Diagram for the EF level positions of the TiO_2 and Ag/TiO_2 under UV light illumination at different temperatures

In the studies performed in solution, C_{60}/C_{60}^- redox potential was used to obtain the equilibrated E_F.[27,28] The undecorated TiO_2 and Au + TiO_2 mixed solutions were firstly illuminated with the UV light for a long time. Then, the light was turned off and C_{60} solution was injected to extract the stored electrons. Under the E_F equilibrium, the E_F of the TiO_2 and the Au+TiO_2 can equilibrate with the redox potential of the C_{60}/C_{60}^-, which could be calculated from the Nernst equation. Their results showed that the redox potential of C_{60}/C_{60}^- for Au + TiO_2 was more negative, based on which a conclusion was obtained that the E_F was closer to the E_{CB} as compared to the pure TiO_2. Similar results were also obtained for Au + ZnO and Ag + TiO_2 system.[27,31] The transfer of the stored electrons from the TiO_2 and Au + TiO_2 to C_{60} could lead to a simultaneous down-shift of the E_F of TiO_2 and Au+TiO_2, when the potential of C_{60}/C_{60}^- was shifted. Therefore, the real E_F should be the sum of the equilibrated redox of C_{60}/C_{60}^- and the E_F down-shift. However, it seems that this study did not take the E_F down-shift into consideration. Because the differential capacitance of the Au+TiO_2 is higher

than that of the space charge region of the TiO_2, the E_F down-shift of Au + TiO_2 must be smaller than that of the undecorated TiO_2. By including this effect, we expected that the E_F of the TiO_2 might be closer to the E_{CB} of TiO_2 as compared to the Au + TiO_2 in these studies; this could agree with our result.

3.3. The electron storage and separation of the Ag nanoparticles

The ΔE_F of an Ag nanoparticle is a function of the charged electron number and the Ag nanoparticle radius according to [51]

$$\Delta E_F = \frac{(2z-1)q^2}{8\pi\varepsilon_0\varepsilon_r R} \quad (6)$$

where ε_0 is the vacuum permittivity, ε_r is relative dielectric constant of the substance surrounding the Ag nanoparticle (~ 1 for air and 48 for anatase TiO_2), R is the Ag nanoparticle radius, and z is the charged (stored) electron number in the Ag nanoparticle. Therefore, the electron storage in an Ag nanoparticle can be estimated based on the ΔE_F before and after light illumination. The porous TiO_2 is composed of air and TiO_2 phases. The dielectric constant of the porous TiO_2 can be estimated from the effective-medium approximation according to the following equation in the 2-dimensional case.[52]

$$f_a \frac{\varepsilon_a - \varepsilon_{eff}}{\varepsilon_a + \varepsilon_{eff}} + (1 - f_a)\frac{\varepsilon_t - \varepsilon_{eff}}{\varepsilon_t + \varepsilon_{eff}} = 0 \quad (7)$$

where f_a, ε_a, ε_t, and ε_{eff} are air volume fraction, air dielectric function, TiO_2 dielectric function, and the effective dielectric constant of porous TiO_2. The BET analysis showed that the porous volume in the TiO_2 is ~22% (Fig. S7). The ε_{eff} was calculated to be 29.5. As the E_F of the TiO_2 and Ag nanoparticles are the same under the quasi-equilibrium approximation, the ΔE_F in eqn (6) corresponds to the ΔE_F of the TiO_2 before and under the steay light illumination.

The numbers of the stored electrons in an Ag nanoparticle under light illumination are estimated to be 46, 47, 47.4 and 47 at 20, 40, 60 and 80 °C, respectively; this shows that the stored electrons are almost independent on temperatures, based on which the density of the stored electrons in the TiO_2 and Ag nanoparticles can be evaluated.

The electrons in the TiO_2 CB can be directly calculated according to Eqn. (2). In addition to the CB states, the electrons can also occupy the band tailed states. Here, the exponentially-distributed gap states distributing below the CB edge [53,54]

$$g(E) = \frac{N_T}{k_B T_0} \exp - \frac{E}{k_B T_0} \quad (8)$$

where N_T is the total trap density, k_BT_0 is the parameter determines the exponential trap depth. The trapped electrons can be calculated according to

$$n_t(E_F) = N_T \int_{-\infty}^{E_{CB}} g(E) f(E, E_F) dE \quad (9)$$

where $f(E, E_F)$ is Fermi-Dirac function. The n_t can be expressed in terms of the hypergeometric function and approximated as [55]

$$n_t = N_t \left[\frac{\pi\alpha}{\sin(\pi\alpha)}\right] \exp - \frac{E_F}{k_B T_0} \quad (10)$$

where α is defined as T/T_0. Supposed the T_0 is 800 K and N_t is 10^{19} cm^{-3}, the density of the stored electrons in the TiO_2 phase were estimated before and after the Ag nanoparticle decoration. The electron storage in the TiO_2 was also estimated when the traps were not included. The number of the Ag nanoparticles loaded over TiO_2 surface are 7.0×10^{15} cm^{-3}. The density (cm^{-3}) of the electrons stored in Ag nanoparticles was also estimated. The result is shown in Table 1. Therefore, it can be seen whether more electrons can be stored in Ag/TiO_2 are related with the electron traps. If the electron traps are not considered, it can be seen that more than 90% of the stored electrons locate at the Ag nanoparticles, independent on the

temperatures**.** When the electron traps are considered, as the electrons can also occupy the traps, so the percentages of the stored electrons in the Ag nanoparticles decreases, and more than 60% electrons are stored in the Ag electrons. Therefore, the electron distribution between the TiO_2 and the Ag nanoparticles is related with the electron traps.

Hirakawa *et al*. used thionine to titrate the electrons stored in Ag/TiO_2 and TiO_2 in methanol-toluene solution, and their result also showed that more electrons were stored in $Ag\text{-}TiO_2$ as compared with the pure TiO_2.[30] Under their experimental condition, ~ 40 electrons can be stored in a 3.7 nm Ag nanoparticle; this is also in good agreement with our result. The result thus shows that the Ag nanoparticles can indeed act as the electron sink, the electrons and holes can be separated at TiO_2 and Ag nanoparticles. In the case of low trap density, the electrons dominantly reside in the Ag nanoparticles, so the Ag nanoparticles can play the role of the reduction sites for photocatalytic reactions. Obviously, the electron storage and distribution in Ag nanoparticles can relates with the Ag nanoparticle size and loaded amount. Therefore, the Ag nanoparticle can effectively separate the charge carriers; this agrees well with our general recognition. We quantitively evaluate the separation in the current research.

Table 1. Density of the electrons residing in Ag nanoparticles and TiO_2 under light illumination at different temperatures (unit: 10^{17} cm^{-3}).

T (°C)	20		40		60		80	
	TiO_2	Ag	TiO_2	Ag	TiO_2	Ag	TiO_2	Ag
Pure TiO_2	7.4 (2.5)[a]		6.3(2.3)		4.4(1.3)		3.7(1.2)	
Ag/TiO_2	2.1 (0.23)	3.2	2.5(0.48)	3.3	2.4 (0.44)	3.3	2.2(0.47)	3.3

[a:] The data in parentheses is the density of the electrons in TiO_2 without considering the electrons traps

3.4. Ag LSPR analysis

In the methanol contained N_2, the TiO_2 and Ag/TiO_2 were selectively excited with a 375 nm laser. The photoinduced holes were quickly captured by the methanol, and the electrons were accumulated in the TiO_2. The resultant Ti^{3+} states and free CB electrons cause a wide absorption from visible to the NIR region.[56] The electron transfer to Ag will affect the electron storage in TiO_2, which might also affect the Ag LSPR in solutions. It is seen that the electron accumulation in TiO_2 leads to a featureless absorption for the TiO_2 under the laser illumination (Fig. S8). The decrease of the absorption after light illumination is ascribed to the electron transfer to the residual O_2; the further exposure to O_2 accelerates the absorption decrease.[57]

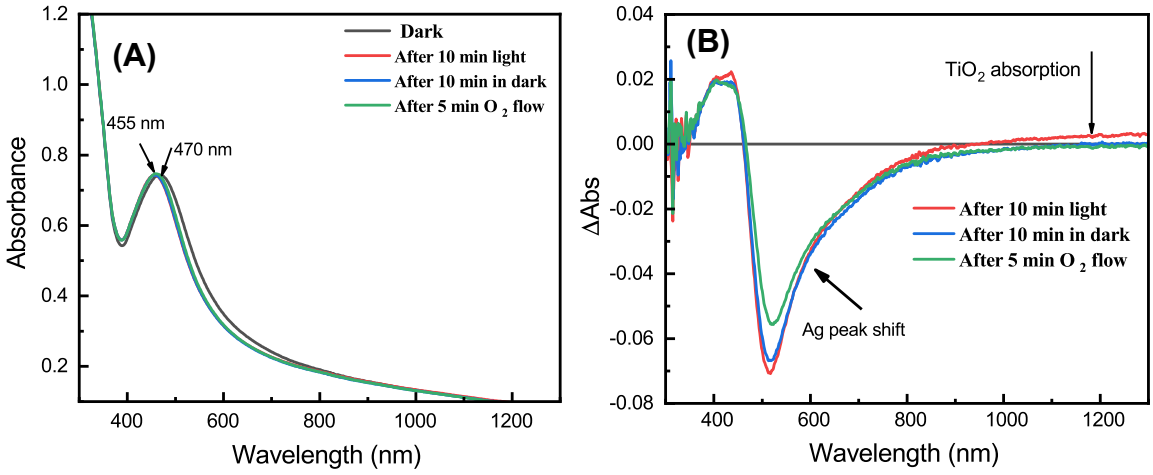

Fig. 7. (A) Absorption spectra of the Ag/TiO_2 before and after 375 nm laser irradiation in methanol contained N_2 under different conditions; (B) Differences of the absorption spectra of the Ag/TiO_2 after light illumination with the dark diffusion spectra before light illumination.

Fig. 7A shows the change of the UV-vis-NIR absorption spectra for the Ag/TiO_2 under different conditions. It can be seen that the laser illumination shifts the Ag LSPR from 470 nm to 455 nm. Subsequent storage of the sample in the dark had almost no effect on the LSPR, the further exposure to O_2 just leads to a very slow LSPR restoration to the initial dark position. The differences of the absorption spectra (Fig. 7B) show that much weaker near-IR absorption (labeled with arrows) was caused by the laser illumination as compared to the TiO_2; this means that less electrons are stored in the TiO_2 phase after the Ag decoration; this is in good accordance with the above conductance analysis. The absorption differences become negative from 450 nm to 880 nm because of the Ag LSPR blue-shift; this also shows that the LSPR almost does not change with time after the end of the laser illumination and the exposure to O_2 has less effect. Therefore, it can be known that the LSPR blue-shift might not arise from the electron storage in the Ag nanoparticles, because it also relates with a change in dielectric environment that might be caused by light illumination. In methanol-toluene solution, the 30 nm blue-shift of the Ag LSPR was observed under UV light illumination, and was attributed to the electron storage in the Ag nanoparticles.[29] As the LSPR restores very slowly after the exposure to O_2, our result cannot support that the UV-light induced LSPR blue-shift is caused by the electron storage.

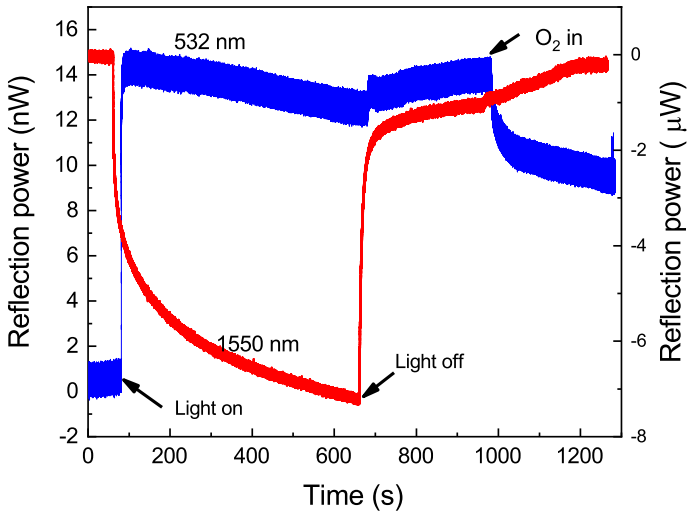

Fig. 8. Evolutions of the diffusion reflectance power at 532 nm and 1550 nm for the Ag/TiO_2 under and after the 375 nm laser illumination in methanol-contained N_2

The E_F equilibrium means there is no electron flux between the Ag nanoparticles and TiO_2 under the steady state, and the E_F of them changes synchronously. As shown in Fig. 7, the change of the diffusion reflectance at 532 nm mainly arises from the LSPR shift, and that at 1550 nm is mainly caused by the electron accumulation in TiO_2. If the electron storage contributes to the LSPR blue-shift, the dynamics change of the photoinduced reflection powers at 532 nm and 1550 nm must be synchronous. Under the 375 nm laser excitation, the time dependences of the *in-situ* diffusion reflectance powers of the Ag/TiO_2 were obtained at 532 nm and 1550 nm in methanol-contained N_2, as shown in Fig. 8. It can be clearly seen that the change of the reflectance power at 532 nm cannot accord with that of 1550 nm. After the end of laser illumination, the fast increase of the reflectance power at 1550 nm means that the stored electrons in the TiO_2 can be quickly consumed and the E_F of the TiO_2 thus experiences a fast decrease, while the unchanged reflectance power at 532 nm indicates that the E_F of the Ag nanoparticles should remain unchanged if the LSPR blue-shift is caused by the electron

storage. Obviously, the observation contradicts with the E_F thermal equilibrium. The above asynchronous dynamics provide the evidences that the physical reason of the LSPR blue-shift is not the electron storage in the Ag nanoparticles.

The LSPR wavelength (λ_i) before the light illumination relates with that (λ_f) after the light illumination through their respective electron number (n_i and n_f) by [58]

$$\frac{\lambda_f}{\lambda_i} = \sqrt{\frac{n_i}{n_f}} \tag{11}$$

According to Fig. 7A, λ_f and λ_i are 455 nm and 470 nm. The electron number is roughly estimated by the following equation in the case of a spherical nanoparticle.

$$n_i = \frac{4}{3}\pi R^3 \times N_b \tag{12}$$

where N_b is the bulk electron density of metallic silver, which is taken as 8.0×10^{22} cm^{-3}, R is the nanoparticle radius. Thus, the n_i in a 10 nm Ag nanoparticle before light illumination is estimated to be ~ 4.2×10^4, and thus the n_f is ~ 4.48×10^4; this means that ~ 2.8×10^3 electrons are stored in an Ag nanoparticle, much higher than the above estimation. Based on Eqn. (6), the ΔE_F of the Ag nanoparticle is 61. 2 eV. It was also reported that one electron charging of a 3 nm Au nanoparticle in solution will lead to a ~ 0.1 eV of ΔE_F; this can accord with our estimation.[59] Parente *et al*. combined Mie scattering and Drude theory to simulate the LSPR blue-shift of the Ag nanoparticles; they found that ~ 3.5×10^4 electrons are needed to be stored in an Ag@TiO_2 core-shell particle to form 5 nm LSPR blue-shift,[32] and ~ 110 eV of ΔE_F can be resulted. So large E_F shift is unphysical and meaningless for the Ag nanoparticles. The above conductance analysis shows that ~ 46 electrons are stored in one Ag nanoparticle, so the LSPR blue shift caused by the electron storage should be too smaller to be seen according to eqn. (11). Therefore, the LSPR blue shift cannot be an indicator of the electron storage in

the Ag nanoparticles. Our result agrees with the conclusion obtained in the study,[32] and is different from that obtained in literatures.[27,29,31]

3.4. The XPS analysis under the in-situ light illumination

The study [32] showed that the reduction of 0.2 nm Ag_2O layer could lead to 5 nm blue-shift of the Ag LSPR, which corresponds to a single-molecular chemical absorption of O_2 over the Ag surfaces, and the reduction of TiO_2 might also have a contribution. However, the above spectroscopic (Fig. 7) results shows that the LSPR blue-shift almost remains invariant when the absorption corresponding the electron accumulation in the TiO_2 phase restored. Therefore, the light induced reduction of TiO_2 should not be the reason causing the LSPR blue-shift. In addition, the slow blue-shift restoration after the exposure to O_2 also does not support that the LSPR blue-shift is caused by the reduction of a thin Ag_2O layer.

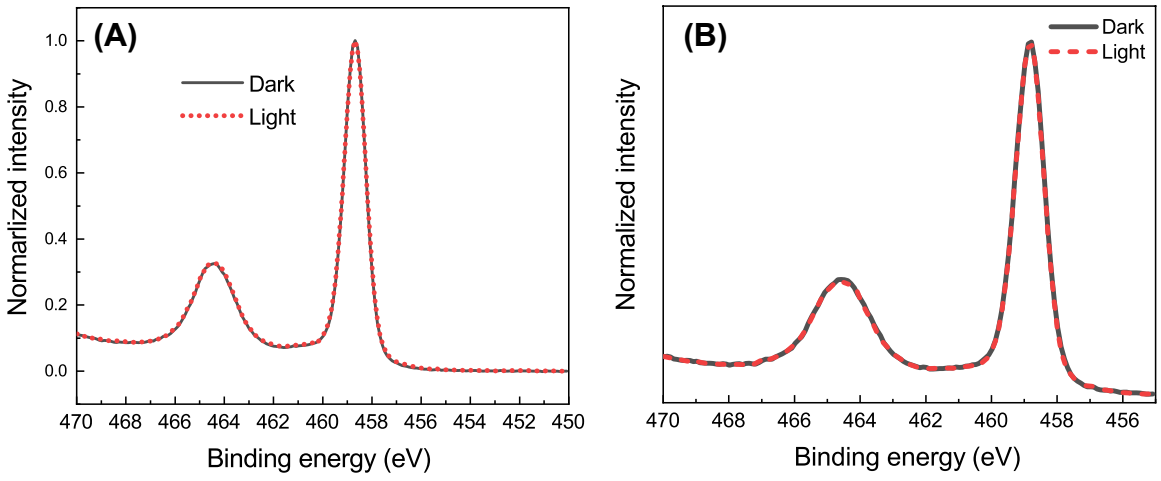

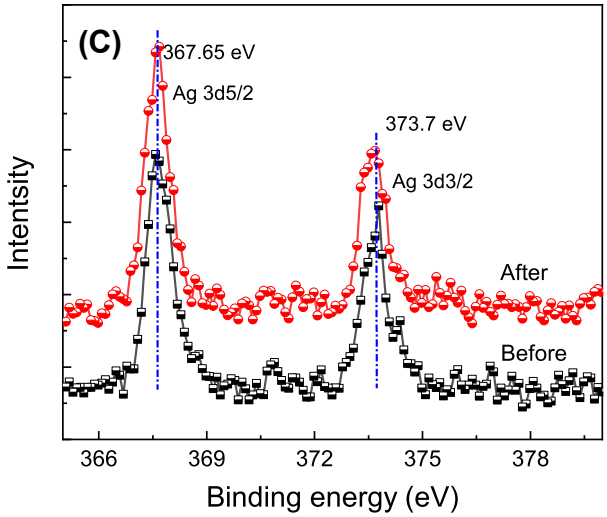

Fig. 9. (A) Ti2p core-level high-resolution XPS spectra of the undecorated TiO2 in the dark and under 375 nm laser illumination; (B) Ti2p core-level high-resolution XPS spectra of the L-Ag/TiO_2 in the dark and under 375 nm laser illumination; (C) Ag3d core-level high-resolution XPS spectra of the L-Ag/TiO2 in the dark and under 375 nm laser illumination

UV light illumination can cause electron accumulation in the Ag/TiO_2 under vacuum. They can transfer to the Ag nanoparticles and reduce the Ag_2O layer. The Ag3d and Ti2p XPS analysis shows that the Ag and Ti surface state are Ag^+ and Ti^{4+} before light illumination, respectively. To check whether the *in-situ* UV light illumination can reduce surface Ti and Ag states, the Ti2p and Ag3d XPS spectra of the methanol pre-adsorbed TiO_2 and Ag/TiO_2 were measured under the *in-situ* 375 nm laser illumination. Fig. 9A shows the Ti2p core-level XPS spectra of the undecorated TiO_2 in the dark and under the 375 nm laser illumination, it can be seen that the electron accumulation does not lead to any observable change in the Ti states. Fig. 9B shows the Ti2p core-level spectra of the Ag/TiO_2 in the dark and under the laser light illumination; this also shows that the Ti states are unaffected by the electron accumulation. The results indicate that the Ti^{3+} state amount is much lower than the intrinsic Ti^{4+} state,

which might not cause an effective change in the dielectric properties of the TiO_2 that can affect the Ag LSPR. It is also seen from Fig. 9C that the laser illumination does not affect the binding energy position of the Ag 3d XPS peaks. It can be also known that the long time UV laser illumination cannot result in a surface reduction of the Ag nanoparticles in the present research. Under the ultra-high vacuum condition during the XPS measurements, although more electrons can be accumulated in the Ag/TiO_2, the chemical states of the Ag and TiO_2 still remain unaffected. Thus, the Ag LSPR blue-shift might not arise from the Ag and TiO_2 reduction; this is different from the conclusion obtained in literatures.[32] Other effect that remains to be discovered may have a contribution.

4. Conclusion

in-situ photoconductances and theoretical analysis were combined to study the E_F and electron separation in the Ag/TiO_2 under gaseous conditions. The results showed that the E_F of the Ag/TiO_2 locates deeper in the gap as compared to that of the TiO_2 under the UV light illumination. It was seen that increasing temperatures had less effect on the E_F of the Ag/TiO_2, while could decrease the E_F of the undecorated TiO_2. It was estimated that ~ 46 electrons can be stored in an Ag nanoparticle under the present experimental condition, which was almost independent on the temperature variation. The role of the Ag nanoparticles in storing and separating electrons should be related to the electron traps in the TiO_2. More than 90% electrons can be stored in the Ag nanoparticles if the electron traps were not considered. It was also revealed that the Ag LSPR blue-shift cannot be ascribed to the electron storage and might also not related with the reduction of Ag nanoparticles and TiO_2. In principle, the method developed in the current research can be also used to study the electron storage and

separation for other metallic nanoparticle decoration, such as Pt, Au, Cu, and Pd. Besides TiO_2, it is also believed that the method is also suitable for other semiconductors such as ZnO, WO_3, and CdS. Therefore, it can be general method that can be used to analyze various nanostructrual systems under in-situ gaseous conditions.

ASSOCIATED CONTENT

Supporting Information: Figures of diffusion spectroscopic cell, EDS of Ag/TiO_2, XRD patterns, XPS spectrum, UV-Vis-NIR diffusion spectra, and the dark V-I curves of the TiO_2 and Ag/TiO_2

AUTHOR INFORMATION

Corresponding author: B. Liu, bshliu@whut.edu.cn

ACKNOWLEDGMENT

B. Liu thanks the National Key research and development of China (No. 2017YFE0192600) and National Natural Science Foundation of China (No. 51772230). L. Wen thanks the Guidance Project of Hubei Provincial Department of Education for Scientific Research (B2020246), Research Fund for the Doctoral Program of Wuhan Technology and Business University (D2019008) and the Special Fund of Advantageous and Characteristic Disciplines (Group) of Hubei Province.

REFERENCES

[1] A. Naldoni, M. Altomare, G. Zoppellaro, N. Liu, Š. Kment, R. Zbořil and P. Schmuki, Photocatalysis with Reduced TiO_2: From Black TiO_2 to Cocatalyst-Free Hydrogen Production, *ACS Catal.*, 2019, **9**, 345–364.

[2] W. Chen, Y. Wang, S. Liu, L. Gao, L. Mao, Z. Fan, W. Shangguan and Z. Jiang, Non-noble Metal Cu as a Cocatalyst on TiO_2 Nanorod for Highly Efficient Photocatalytic Hydrogen Production, *Appl. Surf. Sci.*, 2018, **445**, 527-534.

[3] S. Kreft, W. Duo, H. Jung and M. Beller, Recent Advances on TiO_2-based Photocatalytic CO_2 Reduction, *Energy Chem*, 2020, **2**, 100044.

[4] N. G. Moustakas and J. Strunk, Photocatalytic CO_2 Reduction on TiO_2-Based Materials under Controlled Reaction Conditions: Systematic Insights from a Literature Study, *Chem.-Euro. J.*, 2018, **24**, 12739-12746.

[5] L. Chen, K. Huang, Q. Xie, S. M. Lam, J. Chung Sin, T. Su, H. Ji and Z. Qin, The Enhancement of Photocatalytic CO_2 Reduction by the in-situ Growth of TiO_2 on Ti_3C_2 MXene, *Catal. Sci. Technol.*, 2021, **11**, 1602-1614.

[6] X. Yang, H. Sun, G. Li, T. An and W. Choi, Fouling of TiO_2 Induced by Natural Organic Matters During Photocatalytic Water Treatment: Mechanisms and Regeneration Strategy, *Appl. Catal. B: Environ.*, 2021, **294**, 120252.

[7] T. Xu, H. Zhao, H. Zheng and P. Zhang, Atomically Pt Implanted Nanoporous TiO_2 Film for Photocatalytic Degradation of Trace Organic Pollutants in Water, *Chem. Eng. J.*, 2020, **385**, 123832.

[8] D. A.Panayotov and J. R. Morris, Surface Chemistry of Au/TiO_2: Thermally and Photolytically Activated Reactions, *Surf. Sci. Rep.*, 2016, **71**, 77-271.

[9] S. Linic, P. Christopher, H. Xin and A. Marimuthu, Catalytic and Photocatalytic Transformations on Metal Nanoparticles with Targeted Geometric and Plasmonic Properties, *Acc. Chem. Res.*, 2013, **46**, 1890–1899.

[10] R. Wang, G. Che, C. Wang, C. Liu, B. Liu, B. Ohtani, Y. Liu and X. Zhang, Alcohol Plasma Processed Surface Amorphization for Photocatalysis, *ACS Catal.*, 2022, **12**, 12206–12216.

[11] T. L. Thompson and J. T. Yates Jr. TiO_2-based Photocatalysis: Surface Defects, Oxygen and Charge Transfer, *Topics in Catalysis*, 2005, **35**, 197–210.

[12] K. Nakata and A. Fujishima, TiO_2 photocatalysis: Design and Applications, *J. Photochem. Photobio. C: Photochem. Rev.*, 2012, **13**, 169-189.

[13] Q. Guo, C. Zhou, Z. Ma and X. Yang, Fundamentals of TiO_2 Photocatalysis: Concepts, Mechanisms, and Challenges, *Adv. Mater.*, 2019, **31**, 1901997.

[14] S. Akel, R. Dillert, N. O. Balayeva, R. Boughaled, J. Koch, M. El Azzouzi and D. W. Bahnemann, Ag/Ag_2O as a Co-Catalyst in TiO_2 Photocatalysis: Effect of the Co-Catalyst/Photocatalyst Mass Ratio, *Catalysts*, 2018, **8**, 647.

[15] C. Wang, H. Fan, X. Ren, Y. Wen and W. Wang, Highly Dispersed PtO Nanodots as Efficient Co-catalyst for Photocatalytic Hydrogen Evolution, *Appl. Surf. Sci.*, 2018, **462**, 423–431.

[16] J. Ran, G. Gao, F. T. Li, T. Y. Ma, A. Du and S. Z. Qiao, Ti_3C_2 MXene Co-catalyst on Metal Sulfide Photo-absorbers for Enhanced Visible-light Photocatalytic Hydrogen Production, *Nat. Comm.*, 2017, **8**, 13907.

[17] S. J. P. Varapragasam, S. Mia, C. Wieting, C. Balasanthiran, M. Y. Hossan, A. Baride, R. M. Rioux and J. D. Hoefelmeyer, $Ag–TiO_2$ Hybrid Nanocrystal Photocatalyst: Hydrogen Evolution under UV Irradiation but Not under Visible-Light Irradiation, *ACS Appl. Energy Mater.*, 2019, **2**, 8274−8282.

[18] B. Liu, H. Wu, X. Zhang, I. P. Parkin and X. Zhao, New Insight into the Role of Electron Transfer to O_2 in Photocatalytic Oxidations of Acetone over TiO_2 and the Effect of Au Cocatalyst, *J. Phys. Chem. C*, 2019, **123**, 30958–30971.

[19] C. Dessala, L. Martínez, C. Maheua, T. Len, F. Morfin, J. L. Rousset, E. Puzenat, P. Afanasiev, M. Aouine, L. Soler, J. Llorca and L. Piccolo, Influence of Pt Particle Size and Reaction Phase on the Photocatalytic Performances of Ultradispersed Pt/TiO_2 Catalysts for Hydrogen Evolution, *J. Catal.*, 2019, **375**, 155-163.

[20] R. Zhang, H. Wang, S. Tang, C. Liu, F. Dong, H. Yue and B. Liang, Photocatalytic Oxidative Dehydrogenation of Ethane Using CO_2 as a Soft Oxidant over Pd/TiO_2 Catalysts to C_2H_4 and Syngas, *ACS Catal.*, 2018, **8**, 10, 9280–9286

[21] J. Ivanez, P. Garcia-Munoz, A. M. Ruppert and N. Keller, UV-A Light-assisted Gas-phase Formic Acid Decomposition on Photo-thermo Ru/TiO_2 Catalyst, *Catal. Today*, 2021, **380**, 138-146.

[22] K. Yamanaka, T. Ohwaki and T. Morikawa, Charge-Carrier Dynamics in Cu- or Fe-Loaded Nitrogen-Doped TiO_2 Powder Studied by Femtosecond Diffuse Reflectance Spectroscopy, *J. Phys. Chem. C*, 2013, **117**, 16448−16456.

[23] J. Tang, A. J. Cowan, J. R. Durrant and D. R. Klu, Mechanism of O_2 Production from Water Splitting: Nature of Charge Carriers in Nitrogen Doped Nanocrystalline TiO_2 Films and Factors Limiting O_2 Production, *J. Phys. Chem. C*, 2011, **115**, 3143–3150.

[274] V. Subramanian, E. E. Wolf and P. V. Kamat, Catalysis with TiO_2/Gold Nanocomposites. Effect of Metal Particle Size on the Fermi Level Equilibration, *J. Am. Chem. Soc.*, 2004, **126**, 4943-4950.

[25] M. Jakob and H. Levanon, Charge Distribution between UV-Irradiated TiO_2 and Gold Nanoparticles: Determination of Shift in the Fermi Level, *Nano Lett*., 2003, **3**, 353-358.

[26] T. Hirakawa and P. V. Kamat, Charge Separation and Catalytic Activity of Ag@TiO_2 Core-Shell Composite Clusters under UV-Irradiation, *J. Am. Chem. Soc.*, 2005, **127**, 3928-3934.

[27] T. Hirakawa and P. V. Kamat, Photoinduced Electron Storage and Surface Plasmon Modulation in Ag@TiO_2 Clusters, *Langmuir*, 2014, **20**, 5645-5647.

[28] V. Subramanian, E. E. Wolf and P. V. Kamat, Green Emission to Probe Photoinduced Charging Events in ZnO-Au Nanoparticles. Charge Distribution and Fermi-Level Equilibration, *J. Phys. Chem. B*, 2003, **107**, 7479-7485.

[29] M. Parente, S. Sheikholeslami, G. V. Naik, J. A. Dionne and A. Baldi, Equilibration of Photogenerated Charge Carriers in PlasmonicCore@Shell Nanoparticles, *J. Phys. Chem. C*, 2018, **122**, 23631−23638.

[30] F. Xiao, W. Zhou, B. Sun, H. Li, P. Qiao, L. Ren, X. Zhao, and H. Fu, Engineering Oxygen Vacancy on Rutile TiO_2 for Efficient Electron-hole Separation and High Solar-driven Photocatalytic Hydrogen Evolution, *Sci. China Mater.*, 2018, **61**,822–830.

[31] A. Kumar, A. S. Patel, and T. Mohanty, Correlation of Photodegradation Efficiency with Surface Potential of Silver-TiO_2 Nanocomposite Thin Films, *J. Phys. Chem. C*, 2012, **116**, 20404−20408.

[32] Q. Qiao, X. Zhang, Z. Lu, L. Wang, Y. Liu, X. Zhu, and J. Li, Formation of Holographic Fringes on Photochromic Ag/TiO_2 Nanocomposite Films, *Appl. Phys. Lett.*, 2009, **94**, 074104.

[33] R. Han, X. Zhang, L. Wang, R. Dai, and Y. Liu, Size-dependent Photochromism-based Holographic Storage of Ag/TiO_2 Nanocomposite Film, *Appl. Phys. Lett.*, 2011, **98**, 221905.

[34] Y. Ohko, T. Tatsuma, T. Fujii, K. Naoi, C. Niwa, Y. Kubota, A. Fujishima, Multicolour Photochromism of TiO_2 Films Loaded with Silver Nanoparticles, *Nat. Mater.*, 2003, **2**, 29–31.

[35] K. Naoi, Y. Ohko, and T.Tatsuma, TiO_2 Films Loaded with Silver Nanoparticles: Control of Multicolor Photochromic Behavior, *J. Am. Chem. Soc.*, 2004, **126**, 3664–3668.

[36] Y. Zhu, Y. Liu, Q. Ai, G. Gao, L. Yuan, Q. Fang, X. Tian, X. Zhang, E. Egap, P. M. Ajayan and J. Lou, In Situ Synthesis of Lead-Free Halide Perovskite–COF Nanocomposites as Photocatalysts for Photoinduced Polymerization in Both Organic and Aqueous Phases, *ACS Materials Lett.*, 2022, **3**, 464–471.

[37] J. Xue, S. Jiang, Z. Wang, Z. Jiang, H. Cao, X. Zhu, Q. Zhang, Y. Luo, and J. Bao, Efficient Exciton Dissociation through the Edge Interfacial State in Metal Halide Perovskite-Based Photocatalysts, *J. Phys. Chem. Lett.*, 2023, **6**, 1504–1511.

[38] Y. Hu, D. Li, Y. Zheng, W. Chen, Y. He, Y. Shao, X. Fu, G. Xiao, BiVO4/TiO2 nanocrystalline heterostructure: A wide spectrum responsive photocatalyst towards the highly efficient decomposition of gaseous benzene, Appl. Catal. B: Environ. 2011,104, 30-26.

[39] Z. Hao, G. Wang, C. Da, X. Lv and J. Li, Tuning Photoelectrochemical Performances of Ag-TiO_2 Nanocomposites via Reduction/Oxidation of Ag. *Chem. Mater.*, 2008, **77**, 87-95.

[40] F. Zhang, N. Guan, Y. Li, J. Chen and H. Zhang, Control of Morphology of Silver Clusters Coated on Titanium Dioxide during Photocatalysis. *Langmuir*, 2003, **19**, 8230-8234.

[41] Z. Wu, L. Li, X. Zhou, I. P. Parkin, X. Zhao and B. Liu, A Light–heat Synergism in the Sub-bandgap Photocatalytic Response of Pristine TiO_2: A Study of In Situ Diffusion Reflectance and Conductance, *Phys. Chem. Chem. Phys.*, 2022, **24**, 5618-5626

[42] B. Liu, J. Wang, I. P. Parkin and X. Zhao, The Effect of Cu Dopants on Electron Transfer

to O_2 and the Connection with Acetone Photocatalytic Oxidations over Nano-TiO_2, *Phys. Chem. Chem. Phys.*, 2021, **23**, 8300-8308

[43] Z. Wu, L. Li, X. Zhou, X. Zhao and B. Liu, Kinetics and Energetic Analysis of the Slow Dispersive Electron Transfer from Nano-TiO_2 to O_2 by In Situ Diffusion Reflectance and Laplace Transform, Phys. *Chem. Chem. Phys.*, 2021, **23**, 19901-19910

[44] L. Li, L. Yan, Z. Wu, X. Zhou, X. Zhao and B. Liu, Plasmon-assisted Facile Selective Gaseous Isopropanol Dehydrogenation over Ag Nanocubes, *Catal. Sci. Technol.*, 2022, **12,** 94-104.

[45] G. W. Taylor and J. G. Simmons, Basic Equations for Statitistics, Recombination, Processes, and Photoconductivity in Amorphous Insulaotors and Semiconductors, *J. Non-Cryst. Solids*, 192, **8-10**, 940-946.

[46] J. A. Freire and G. A. Emidio, What can Transient Absorption Spectroscopy Reveal about the Trap Distribution in a Semiconductor? *J. Photochem. Photobio. A: Chem.*, 2020, **393**, 112439.

[47] H. Tang, K. Prasad, R. Sanjinbs, P. E. Schmid and F. Levy, Electrical and Optical Properties of TiO_2 Anatase Thin Films, *J. Appl. Phys.*, 1994, **75**, 2042

[48] B. Liu, X. Zhao, J. Yu, I. P. Parkin, A. Fujishima and K. Nakata, Intrinsic Intermediate Gap States of TiO_2 Materials and Their Roles in Charge Carrier Kinetics, *J. Photochem. Photobio. C: Photochem. Rev.*, 2019, **39**, 1-57.

[49] K. Sakaguchi, K. Shimakawa and Y. Hatanaka, Dynamic Responses of Photoconduction in TiO_x Films Prepared by Radio Frequency Magnetron Sputtering, *Jpn. J. Appl. Phys.*, 2010, **49**, 091103.

[50] K. Sakaguchi, K. Shimakawa and Y. Hatanaka, Photoconductive Characteristics of Hydro-Oxygenated Amorphous Titanium Oxide Films Prepared by Remote Plasma-Enhanced Chemical Vapor Deposition, *Jpn. J. Appl. Phys.*, 2006, **45**, 4183–4186.

[51] M. D. Scanlon, P. Peljo, M. A. Mrndez, E. Smirnova and H. H. Girault, Charging and Discharging at the Nanoscale: Fermi Level Equilibration of Metallic Nanoparticles, *Chem. Sci.*, 2015, **6**, 2705.

[52] H. S. Choi, J. S. Ahn, J. H. Jung, T. W. Noh and D. H. Kim, Mid-infrared Properties of a VO_2 Film near the Metal-insulator Transition, *Phys. Rev. B*, 1996, **54**, 4621-4628.

[53] B. Liu, Monte-Carlo Modelling of Nano-material Photocatalysis: Bridging Photocatalytic Activity and Microscopic Charge Kinetics, *Phys. Chem. Chem. Phys.*, 2016, **18**, 11520-11527

[54] B. Liu, X. Zhao, J. Yu, A. Fujishima and K. Nakata, A Stochastic Study of Electron Transfer Kinetics in Nano-particulate Photocatalysis: A Comparison of the Quasi-equilibrium Approximation with a Random Walking Model, *Phys. Chem. Chem. Phys.*, 2016, **18**, 31914-31923.

[55] M. Tachiya and K. Seki, Theory of Bulk Electron-hole Recombination in a Medium with Energetic Disorder, *Phys. Rev. B*, 2010, **82**, 085201.

[56] T. Yoshihara, R. Katoh, A. Furube, Y. Tamaki, M. Murai, K. Hara, S. Murata, H. Arakawa and M. Tachiya, Identification of Reactive Species in Photoexcited Nanocrystalline TiO_2 Films by Wide-Wavelength-Range (400-2500 nm) Transient Absorption Spectroscopy, *J. Phys. Chem. B*, 2004, **108**, 3817-3823.

[57] N. M. Beekma, Effect of Oxygen Chemisorption and Photodesorption on the Conductivity of ZnO Powder Layer, *J. Chem. Soc., Faraday Trans*, 1978, **74**, 31-45.

[58] A. C. Templeton, J. J Pietron, R. W. Murray and P. Mulvaney, Solvent Refractive Index and Core Charge Influences on the Surface Plasmon Absorbance of Alkanethiolate Monolayer-Protected Gold Clusters, *J. Phys. Chem.* B, 2000, **104**, 564

[59] S. Chen, R. S. Ingram, M. J. Hostetler, J. J. Pietron, R. W. Murray, T. G. Schaaff, J. T. Khoury, M. M. Alvarez and R. L. Whetten, Gold Nanoelectrodes of Varied Size: Transition to Molecule-like Charging, *Science*, 1998, **280**, 2098.